Global Journal of Science Frontier Research: H
Environment & Earth Science
Volume 23 Issue 3 Version 1.0 Year 2023
Type: Double Blind Peer Reviewed International Research Journal
Publisher: Global Journals
Online ISSN: 2249-4626 & Print ISSN: 0975-5896

Kinetics of the Water Release of Hygroscopic Acrylamide Gel Embedded in Calcium Chloride by Thermogravimetric Analysis

By Nasrollah Hamidi, India Williams & Hushmand Hamidi

South Carolina State University

Abstract- Poly (acrylamide) gel was synthesized by radical polymerization of acrylamide and N, N'- methylene-bisacrylamide in the presence of benzoyl peroxide and carbon nanotubes. The dry product was saturated with calcium chloride and prepared for water absorption and desorption. The kinetics of water desorption of poly (acrylamide) gel embedded with hygroscopic calcium chloride (DHG), was studied from thermograms data of thermogravimetric analysis (TGA).

DHG captures vapor from the environment and releases it as fresh water; it can be used as the condenser to build atmospheric water generators (AWGs) to alleviate the freshwater stress rusting from innovative activities such as industrial, agricultural, rural, and defense endeavors. The kinetics parameters of the synthesized DHG showed that it absorbed environmental vapor at room temperature and released water below its boiling point (40 to 90 °C), temperatures achievable under sunlight via the photothermal effect.

Keywords: steam harvesting, dew collection, freshwater, desiccants, thermoresponsive gel, activation energy, spontaneous water release.

GJSFR-H Classification: LCC: TP155-TP156

Strictly as per the compliance and regulations of:

Kinetics of the Water Release of Hygroscopic Acrylamide Gel Embedded in Calcium Chloride by Thermogravimetric Analysis

Nasrollah Hamidi [α], India Williams [σ] & Hushmand Hamidi [ρ]

Abstract- Poly (acrylamide) gel was synthesized by radical polymerization of acrylamide and N, N'- methylene-bisacrylamide in the presence of benzoyl peroxide and carbon nanotubes. The dry product was saturated with calcium chloride and prepared for water absorption and desorption. The kinetics of water desorption of poly (acrylamide) gel embedded with hygroscopic calcium chloride (DHG), was studied from thermograms data of thermogravimetric analysis (TGA).

DHG captures vapor from the environment and releases it as fresh water; it can be used as the condenser to build atmospheric water generators (AWGs) to alleviate the freshwater stress rusting from innovative activities such as industrial, agricultural, rural, and defense endeavors. The kinetics parameters of the synthesized DHG showed that it absorbed environmental vapor at room temperature and released water below its boiling point (40 to 90 °C), temperatures achievable under sunlight via the photothermal effect. In this work, the energy barrier of DHG to release water (Ea) was evaluated from thermogravimetric measurements using the isoconversional method. The values of Ea varied with temperature; it was highest at t ~ 40 °C, and became negligible and negative at t < 50 °C, indicating that the water release was not required extra energy. The water release rate was increasing with temperature showing a maximum rate around 75-89 °C.

Keywords: steam harvesting, dew collection, freshwater, desiccants, thermoresponsive gel, activation energy, spontaneous water release.

I. Introduction

Earth contains 1,386 million cubic kilometers (Mckm) of water, composed of 35.5 Mckm (2.5 %) freshwater, where less than 0.75% of it is sustainably managed, and its resources are diminishing by the progress of civilization, causing water anxiety throughout the world. [1] The water stress would be alleviated far and wide, by harvesting the renewable, invisible atmospheric vapor (equivalent to 12,900 cubic kilometers of liquid water), by developing "atmospheric water generators" (AWGs). [2,3] In some arid and humid areas of Asia, America, and Africa, fog collectors and AWGs have been installed to alleviate local water stress and prevent forced immigration and poverty. [4–6]

Water calamity - resulting from climatic conditions, wars, urbanization, excess usage, natural and industrial pollution- is among the 5th global risk that impacts societies and the lives of almost 11% of Earth's population. [7–10] It is estimated that by 2050 nearly half of the world's population will be stressed for clean water, [8, 11] including 40 out of 50 USA States. Worldwide, potable water accelerated consumption continues to increase thrice within the last 50 years. [12,13] Food production withdraws over 74% of water, and; a 14% increase in food production and water withdrawal was predicted by 2030. [14–16] Desalination of seawater and inland saline water, [17–19] could alleviate water stress for more than 4 billion people [20] who live in salty regions.[21] Moreover, mineral contamination is a fundamental problem in many places, such as 50 countries living in the Pacific Ring of Fire. [22] The availability of individual AGW units working with the forces of nature would alleviate many water-stressed situations.

The amount of steam, the third most abundant gas in the Earth's atmosphere (~1-3%, depending on location), [23] is measured as the percent of relative humidity (% RH), and its concentration depends on the location, time, temperature, geographic and climatic conditions. [3, 24] A warmer atmosphere holds more moisture- about 7 percent more per 1°C of warming. These changes cause dewfall as a natural water source for plants and animals, particularly in arid and humid regions. Dew collections are also used for human consumption as AWGs become more popular. [25] Active AWGs require a significant heat release, and their mechanism is more thermodynamically complicated than passive AWGs and fog harvesters. [18, 26–29]

II. Progresses in the Field

The development of stimuli-responsive polymeric materials that exhibit controllable wettability in response to external stimuli has contributed to the success of atmospheric water generators (AWGs). For example, temperature-responsive polymers regulate

Corresponding Author α: Department of Biological and Physical Sciences/1890-Research, South Carolina State University, Orangeburg, SC 29117 USA. e-mail: nhamidi@scsu.edu
Author σ: Undergraduate Student, Department of Biological and Physical Sciences/1890-Research, South Carolina State University, Orangeburg, SC 29117 USA.
Author ρ: High school student, Department of Biological and Physical Sciences/1890-Research, South Carolina State University, Orangeburg, SC 29117 USA.

water condensation and release at the molecular level by a phase transition from hydrophilic to hydrophobic, as a response to the changes in temperature. When these polymers are incorporated into an interpenetrating polymeric gel network, they can capture moisture from the air at lower temperatures and release water through a phase separation process at slightly higher temperatures. Stimuli-responsive polymers that have been used for this purpose include poly (acrylamide) [29], poly (N-vinyl caprolactone) [30], poly (N, N-diethylamino ethyl methacrylate), Poly (pyrrole chloride) (PPy-Cl)[31], poly(N-isopropyl acrylamide) (PNIPAM)[32] and some copolymers such as poly (L-lactic acid)−poly(ethylene glycol)−poly (L-lactic acid), [33] These materials exist in a hydrophilic state in which they absorb environmental water quickly, but they can be controllably switched to a hydrophobic state to release the water they contain without the need for energy-intensive processes. This behavior has led to the creation of responsive nanostructured polymer materials and systems, including thin films, particulates, and assemblies, that offer a new opportunity for AWG development. Intelligent materials, alone or combined with hygroscopic minerals and hygroscopic polymers, have provided an effective moisture absorption and desorption network. [34]

PNIPAM is one such stimuli-responsive polymer that undergoes a phase transition at its lower critical solution temperature (LCST), which is around 32 °C. [32] Hair-sized fibers made of a mixture of hydrophobic plastics and hydrophilic PNIPAM have been shown to capture water from a highly humid atmosphere at lower temperatures (below 25 °C) within a few minutes and release it at temperatures above 35 °C. [32] The amounts of thermoresponsive PNIPAM in the skin layer controlled the wettability of the fibers. Other hydrophilic polymers, such as nylon, have also been effective when electro-spared on the surface of the fibers. Similarly, a combination of PNIPAM with hydrophilic sodium alginate has been shown to create an interpenetrating polymer network gel that can capture moisture from the air and deliver liquid water directly. [5, 35–37]

Metal-organic frameworks (MOFs), which result from reticular chemistry, are another kind of three-dimensional interconnected network of highly porous crystalline solid materials suitable for AWGs fabrication. [23, 38, 39] The desorption process requires heat input depending on the water molecules' adsorption strength to reach regeneration temperature, ranging from 70 to 170°C. [18, 40]

Hygroscopic minerals, such as calcium chloride, lithium chloride, lithium bromide, silica gel, and zeolite, are also effective in attracting moisture everywhere, in very low and highly humid environments. [5, 41–45] These moisture absorbents have been used to fabricate AWGs that harvest moisture at night when the worm air gets cold and its humidity increases. The water desorption occurred during the day by heating the hygroscopic bed with solar radiation in a closed container. [5] In contrast to the conventional method of extracting water from dry, arid environments, this process requires less energy since, in the dry and arid regions experiencing a 20% RH at 30 °C, an energy-intensive and impractical process must cool the air to below its dew point (~ < 4 °C) to turn vapor into liquid. However, by heating the humid descants in a closed container, air humidity reaches above 80% RH at 30 °C in the cabin, then the vapor liquefied at temperatures below the dew point (below 26 °C). This process requires less energy than extracting water from any dry and arid environments. [46, 47]

This study presents the preparation and process of absorption and desorption of a poly (acrylamide) hydrogel sample using TGA and DSC. The highest desorption rate temperature and its energy barrier were estimated. The effectiveness of the hydrogel in obtaining water from the environment and fabricating AWGs has been previously studied by other researchers.[29] The obtained values were consistent with expectations and supported the findings in the existing literature. This research occurred under natural environmental conditions, not a controlled environment and artificial simulations.

III. Experimental

a) Materials

Carbon nanotubes (CNTs), nitric acid, sulfuric acid, acrylamide (AA), N, N'-methylene bis acrylamide (MBAA), and benzyl peroxide were purchased from Fisher Scientific, a Thermo Fischer Scientific (USA) company. They were used as received. Fresh distilled water was prepared in the lab.

b) Synthesis

5 mL of distilled water, 1 g of acrylamide (AA), 0.85 mg of N, N'-methylene-bis- acrylamide (MBAA) as a crosslinker, 0.56 mg of benzyl peroxide as the polymerization initiator, and 220 mg of CNT as solar heat absorbent were added to a 60 mL ThermoScientific™ screwed cap septum vials. The mixture was held for 30 min under a stream of 30 mL.min-1 ultrapure argon to eliminate the oxygen present, then kept in an ultrasound bath for 2 hours. The mixture was incubated at 60 °C for a day to polymerize. The obtained hydrogel sample was freeze-dried for 24 hours; then it was immersed in a 1 M solution of CaCl2 for 24 hours under laboratory conditions. The saturated sample of hydrogel (DHG) was dried in an oven at 80 °C for a week. Water absorption of the DHG in the outside environment was not studied, and the desorption of water from the DHG by sunlight was also not explored.

c) Thermogravimetric Analysis (TGA)

The TGA studies were conducted on a TGA-7 Thermogravimetric Analyzer (PerkinElmer, Inc., USA) controlled by Pyrus 13.2.3 software on a Dell PC. The instrument was calibrated using a four-point calibration method since the thermocouple in this device is not in direct contact with the sample. The absorption reaction was prevented by increasing temperature linearly and a well-controlled nitrogen stream of 60 mLmin-1 (room temperature and atmospheric pressure), which carried the volatiles away as soon as they formed. The sample weight preserved was recorded continuously with the corresponding temperature and time. To accurately determine the kinetics parameters, several scans were carried out at different heating rates (β), including 0.5, 1, 2, and 5 Kmin-1. After each scan, the sample was exposed to the lab environment for a few days to saturate with vapor. The data were downloaded to Microsoft Excel for analysis. The values of the extent of desorption (α) for each sample were estimated by (100-%Wi)/100, where % Wi represents the normalized weight of the remaining sample. The values of α increase from zero to the extent that the dehydration occurred, instead of to one, as the dehydration progressed from initiation to completion, respectively.

d) Differential Scanning Calorimetry (DSC)

The DSC experiments were performed using a DSC-7 Differential Scanning Calorimeter (PerkinElmer, Inc., USA) under a stream of argon gas at a flow rate of 60 mLmin-1. The instrument was operated using Pyrus 13.2.3 on a Dell PC. The instrument was calibrated using a standard sample of indium. A well-dried DHG aliquot was crashed and blended in a mortar and pestle before inserting it into an aluminum DSC pan for thermal analysis.

IV. Results and Discussions

a) Water Sorption Experiments

The environmental vapor sorption test was conducted on a Mettler-Toledo Balance at the laboratory conditions of 28 °C, 57% RH during July 2022, in Hodge Hall Lab 314. About 1 g of the previously generated DHG was placed on the scale to monitor its water absorption capacity through weight measurement over three days, as shown in Fig. 1. As time progressed, the weight of the DHG increased, indicating that water was being absorbed into the hydrogel from the environment. The DHG absorbed water over 20% of its weight water in, during 7.5 hours (hs), 50% of its weight after 28hs, and over 60% of its original weight when exposed to the lab environment for 50 hours. The rate of moisture absorption by the hydrogel decreased over time. The initial moisture absorption rate was 0.042%/h; it became slower on the second day (0.022%/h), and much slower on the third day (0.012 %/min) of the environmental exposure.

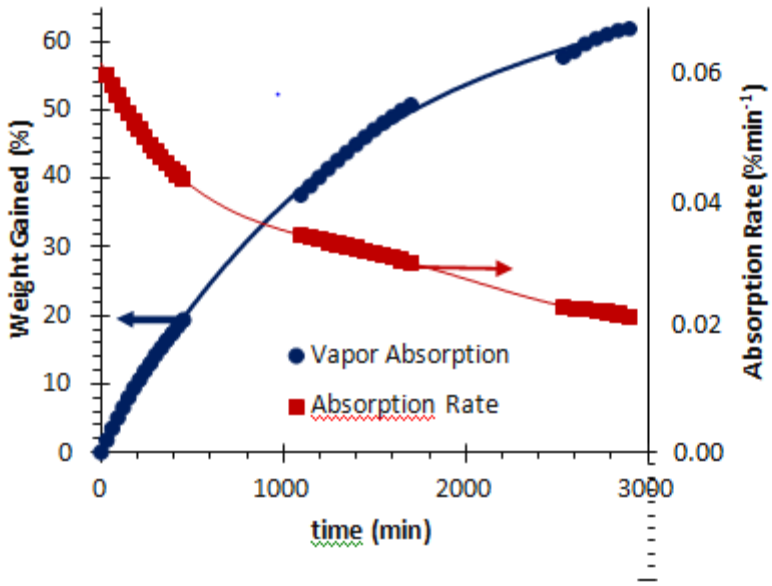

Fig. 1: Variation of the Hydrogel Weight and the Water Absorption Rate.

b) Photo-Thermal Bath

Charcoal was taken as an example of photothermal absorbent material assuming that its photo absorption is similar to as that of the CNTs. The temperature increase of the charcoal was monitored every 5 mins interval, using an infrared thermometer, from 10 AM to 1 PM on a sunny day (June 2022) when the highest daily temperature was 36 °C. Initially, the charcoal absorbed solar heat at a very high rate; however, after 50 min, the temperature changes plateaued, as shown by the graph in Fig. 2.

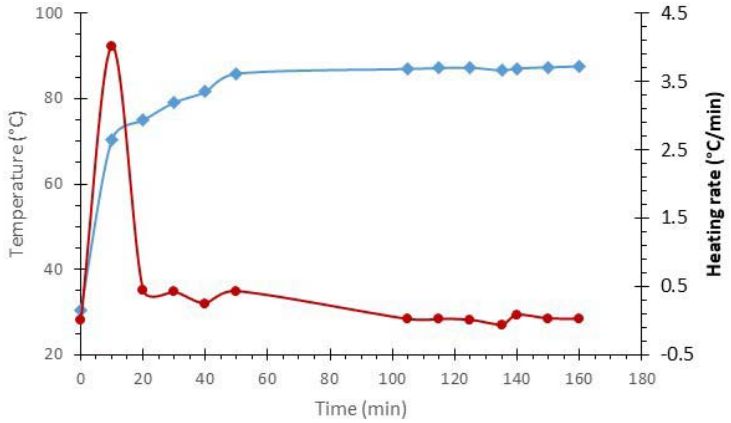

Fig. 2: A Graphical Representation of the Change in Charcoal Temperatures under Direct Sunlight in an Aluminum Box.

c) Differential Scanning Calorimetry (DSC)

The physical properties such as melting point (mp) and glass transition temperature (Tg) are significant properties of solid materials since they determine their industrial application and the types of processing. Polyacrylamide (PAA) has a relatively high melting point (>300 °C) and glass transition temperature (~163 °C) due to strong polar interactions between its amide groups. During the first DSC scan of the DHG (Fig. 3) physical changes at temperatures ~ 50. °C (ΔH ~ 22.7 Jg-1), and 179 °C (ΔH ~ 371 Jg-1) were observed. These transitions are not related to PAA's melting point or glass transition temperature, nor are they related to the melting point of acrylamide (84.5 °C). We can, therefore, conclude that they are related to the new product, DHG, as expected.

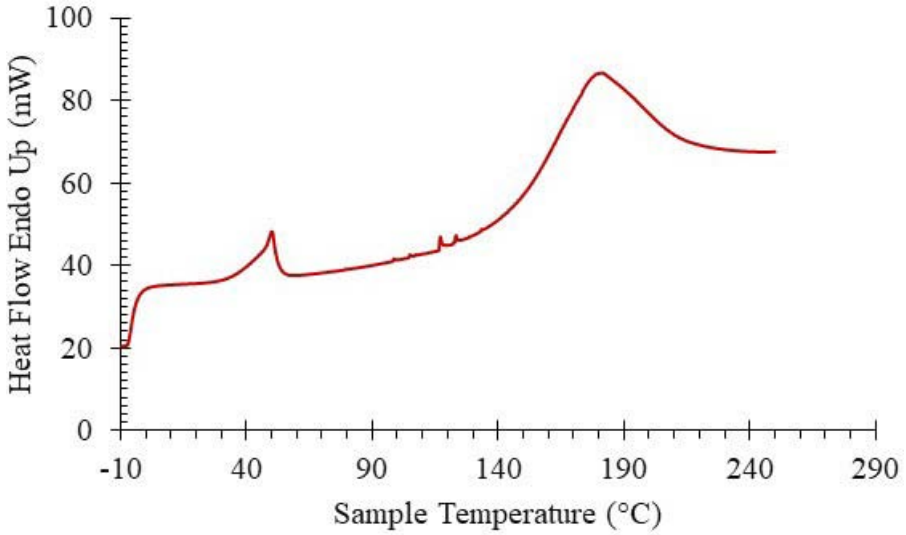

Fig. 3: Thermogram of Differential Scanning Calorimetry (DSC) of a Sample (27.73 mg) of DHG at the β =10 $Kmin^{-1}$

The transition that initiated around 35 °C and maximized around 50 °C could be related to a phase transition and conformational rearrangements of PAA gel. This thermal transition could also be responsible for the spontaneous release of absorbed vapor in the form of liquid water at temperatures above 50°C as observed by TGA measurements documented in the next sections.

d) Thermogravimetry Studies

A TGA pan was loaded with 32 mg of dry hydrogel for water desorption analysis. The sample was left at room condition for three days to absorb humidity, and then subjected to TGA testing. The water desorption was initiated as soon as the sample was placed into the TGA pan (27-30 °C), as shown by the TGA thermograms in Fig. 4. The 3rd and 4th scans were made after the sample was regenerated for a few days in the lab. The

DHG released about 24% of the absorbed water during the first scan. The second scan was taken a few hours after the first scan when the sample had lost most of its absorbed water and did not have enough time to regenerate.

The upper section of Fig. 4 shows the water desorption thermograms and the lower section shows the dehydration rates. In all scans, the water desorption was initiated slowly; its rate increased progressively as temperature increased, and reached maximum around 79 °C, a temperature below the boiling point of water (100 °C). Our results are consistent with previous studies, which have also reported the release of water from DHG below the water's boiling point. [29]

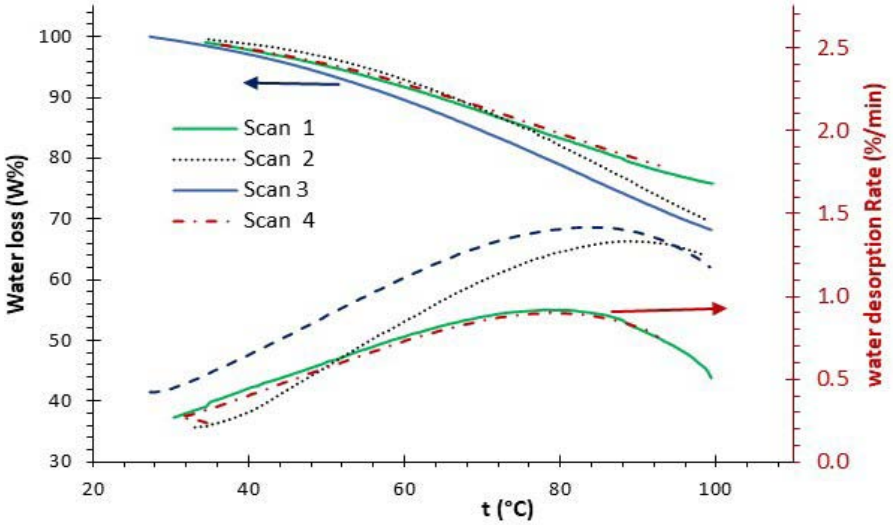

Fig. 4: (Top) Thermograms of Water Desorption and (Bottom) the Water Desorption Rate of the DHG from Room Temperature to 100 °C.

e) Kinetics of Water Desorption

The kinetics of the thermally simulated dehydration of the deliquescent hydrogel (DHG) was studied by the measurement and parameterization of the rates of weight loss originating by eq.1: [48]

$$DHG(\ active\ ) \xrightarrow{\Delta} DHG + H\ \ 2O\ (vapor) \qquad (1)$$

Moist DHG (active) was heated ($\xrightarrow{\Delta}$) to release the absorbed humidity in the form of vapor [H2O (vapor)] or nano-droplets of water that were carried away with a 60 mLmin-1 stream of nitrogen. The rate of thermally stimulated dehydration of DHG (-dW/dt) is expressed by the negative derivative of the TGA thermogram data (-DTGA) of dehydration initiated by the changes in temperature. The rate of dehydration is parameterized by the advancement of dehydration (α) where (1-α) represents the residual amount of DHG(active), the mechanism of reaction expressed by f (α) function (Table 1) and the Arrhenius rate constant [k(T)], as shown by Eq. 2: [49–55].

$$Rate = \frac{d(1-\alpha)}{dt} = -k(T).f(\alpha) \qquad (2)$$

Where T represents the absolute temperature value in K, Ea represents the energy barer to release water by the DHG, and R = 8.314 J mol-1 K-1 is the universal gas constant. Equation (2) is the starting point for various differential kinetic methods and applies to any reaction type.

The values of E_a, and lnA, with the pre-assumed form of f (α), are estimated from the slope and intercept of the Arrhenius plot based on eq. 3, (ln [Rate/f(α)] = ln k versus 1/T) as shown in Figs. 5, for each given α values, respectively.

$$ln\left[-\frac{dw/dt}{f(\alpha)}\right] = ln\left[\frac{\frac{d\alpha}{dt}}{f(\alpha)}\right] = ln\ k = -\frac{E_a}{RT} + ln\ A \qquad (3)$$

The TGA data were analyzed using Eq. 3, which provides information on the weight, temperature, and rate of weight loss at each interval. The isoconversional method, which assumes that the mechanism of a reaction remains the same at a given α value regardless of the heating rate, was used to construct the Arrhenius plot for a given α value. This work using the pre-assumed models expressed by f (α) functions (see Table 1 for details). The Arrhenius plots for the dehydration of the DHG according to each f (α) are shown in Fig. 5, with the x-axis representing the reciprocal of temperature (in Kelvin) and the y-axis representing the natural logarithm of the ratio of the dehydration rate and a given f (α) function. The slope of the adjusted line to the data represents the value of the activation energy divided by the gas constant (Ea/R). As expected, a negative slope of the adjusted line to the experimental data indicates an endothermic activation

energy barrier. The pre-assumed models, f (α) values used in this work are shown in Table 1. If the data shows a positive slope, this indicates that there is no energy barrier for dehydration; and that the reaction is self-activated and spontaneous. This phenomenon was observed for some of the extent of reactions as shown in lines of Fig 4.

Table 1: Set of *f* (α) Functions that were used as Reaction Models to Describe the Thermally Stimulated Water Release of the Deliquescent Hygroscopic Hydrogel System (DHG).

No.	Reaction Model	Code	*f* (α)
1	Power law	P4	$_{4}\alpha^{3/4}$
2	Power law	P3	$_{3}\alpha^{2/3}$
3	Power law	P2	$_{2}\alpha^{1/2}$
4	Power law	P2/3	$_{2/3}\alpha^{-1/2}$
5	One-dimensional diffusion	D1	$1/2\alpha^{-1}$
6	Mampel (first order)	F1	$(1-\alpha)$
7	Avrami–Erofeev	A4	$4(1-\alpha)[-\ln(1-\alpha)]^{3/4}$
8	Avrami–Erofeev	A3	$3(1-\alpha)[-\ln(1-\alpha)]^{2/3}$
9	Avrami–Erofeev	A2	$2(1-\alpha)[-\ln(1-\alpha)]^{1/2}$
10	Three-dimensional diffusion	D3	$3/2(1-\alpha)^{2/3}[1-(1-\alpha)^{1/3}]^{-1}$
11	Contracting sphere	R3	$3(1-\alpha)^{2/3}$
12	Contracting cylinder	R2	$2(1-\alpha)^{1/2}$
13	Two-dimensional diffusion	D2	$[-\ln(1-\alpha)]^{-1}$
14	Random Scission	L2	$2(\alpha^{1/2}-\alpha)$

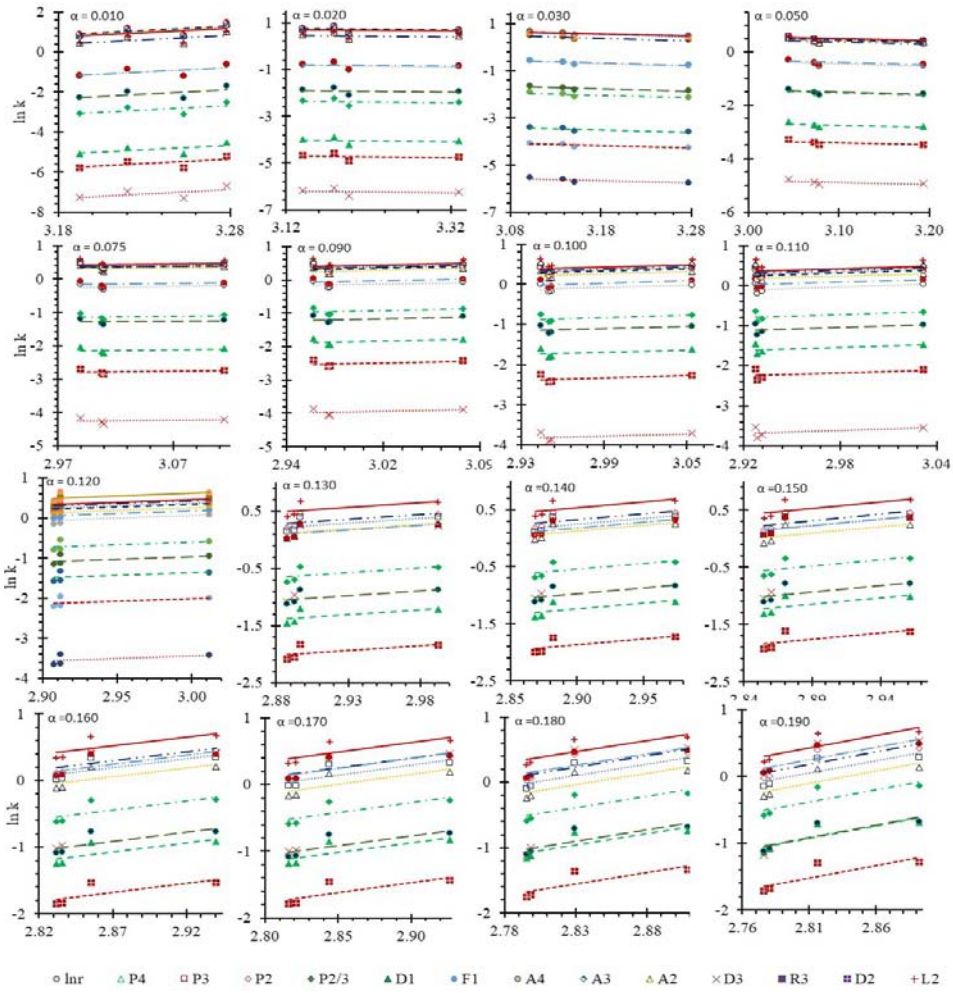

Fig. 5: Arrhenius Plots of the Deliquescent Hygroscopic Hydrogel (DHG) Dehydration at the Given α values.

Fig. 5 represents the Arrhenius plots, according to the isoconversional method, for each indicated α value. The energy barrier for each extent of reaction was obtained for the slope of the corresponding plot are shown in Fig. 6.

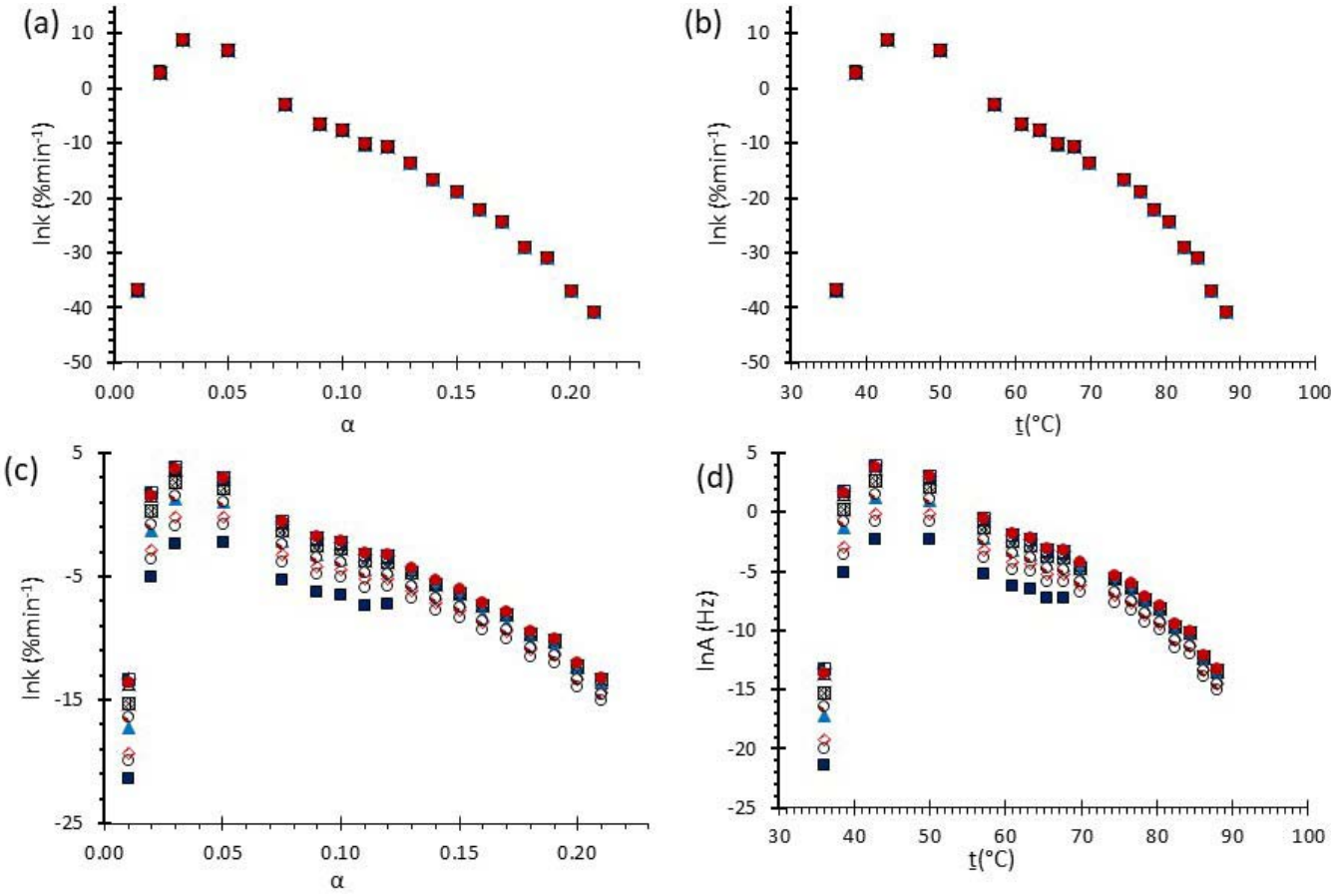

Fig. 6: Variation of (a) Activation Energy Barrier of Dehydration (Ea) and (c) Values of Arrhenius Pre-Exponential Factor (lnA) of DHG Versus the Corresponding Extent of Reaction (α), Respectively; and (b) Ea and (d) lnA of DHG Versus the Corresponding Average Temperatures (t), Respectively.

Figure 6 (a) represents the energy barrier values obtained by applying the isoconversional method for each α value (Ea, α) using the reaction models enlisted in Table 1, where the values of α ranged from 0.010 to 0.210. The corresponding lnA values are shown in Fig. 6(c); the corresponding r2 values are shown in Fig. 7. For a given value of α, the estimated values of Ea, α obtained from the slopes of the adjusted lines were found to be closed to each other, independent of the f(α) function, as expected. For instance, the average values of the Ea, α obtained from the slopes of all models for α = 0.075 was Ea, 0.075 = -2.88 ±0.01 kJmol-1 with the corresponding lnAα = 1.70 ± 1.48 and for α = 0.120, the Ea, 0.120 = -10.70 ±0.01 kJmol-1, with the corresponding lnAα = -4.22 ± 1.19. However, the variations of the values of lnAα depended on the f(α) function, as expected.

The nature of the isoconversional method leads to the fact that at a given α value each thermogram possesses its own reaction rate and temperature; therefore, there is not a given temperature value for a given α value. To evaluate the variations of kinetics parameters by temperature, the approach was to take the average temperature value (t) for each α. The variation of Ea, α and lnAα values with corresponding average temperatures are shown in Fig. 6 (b) and (d), respectively. A comparison of Figs. 6 (a) and (b) shows that the values of Ea, α have similar trends indicating the average temperature approach is acceptable. Similar trends were observed for the variations of lnAa versus α and t as shown by Figs 6 (b) and (d). Moreover, variations of both Ea, α and lnAα versus α and t have shown a similar trend, indicating their interdependence behavior, as was expected. These values, most likely, are composite values, determined by the sum of activation energy barriers of the involved individual steps by assuming that the water delivery has the Arrhenius temperature dependency. [50, 56, 57] These values are called "effective," "apparent," "empirical," or "global," and they are different from intrinsic parameters. The effective activation energy can vary strongly with the temperature and the extent of conversion [58–60] or

take on negative values. [61] Such discrepancies are not expected for the E_a values of a single-step chemical reaction or a physical change. As the reaction progressed, the Ea, α of DHG followed its paths according to the nature of the reaction models and reactants, as shown by the graphs in Fig. 6 (a & c).

The approach to evaluating independently Aα and f (α) in a model-free method was explained in detail by other authors. [62–64] These studies emphasized correlations between the reaction rate, activation energy, pre-exponential factors, and changes in the rate-limiting steps of the individual steps of a chemical reaction. Since the rate of reaction (Rα) at a given α value is expressed as the product of two terms, [Aα f (α)] and [exp (−Eα/RT)], therefore, as the value of Rα decreases and one of the two terms increases the other decreases. When the term, Eα, becomes dominant, it is a sign of a change in the limiting step of the reaction.

The values of Ea of the DHG sample increased with increasing temperature. They reached a maximum value of ~45 °C as indicated in Fig. 6(b). They continuously descended till the end of the dehydration process, as shown in Fig. 6. The highest energy barrier of dehydration of DHG was at the temperature range of 39-50 °C. This behavior is expected since the DHG spontaneously absorbs moisture from the environment at temperatures below 40 °C and releases it at temperatures above 40 °C. The sample weight loss started as soon as it was placed in the TGA pan, where the easy-access water was removed by the high nitrogen flow (60 mL. min-1) passing into the system. The increase of Ea in the plot by increased temperatures is due to reducing the amounts of easy-to-arrest surface water. The highest value of Ea required to release water was around 10 kJmol-1 at 45 °C; which is a very low amount of energy and easily achievable. At temperatures above 50 °C, the amounts of Ea were decreased by increasing the temperature, indicating that the DHG easier release water at moderately low temperatures (t > 50°C), which is achievable by sunlight as shown in Fig. 2. The moisture release is due to the phase transition of the polymer gel which causes the released of stored water spontaneously. The conformational transition of the DHG was also confirmed by DSC measurements as shown in Fig. 3

Figure 7 shows the values of r2 when the experimental data were fit into a given α value for a corresponding f(α) models listed in Table 1. The dehydration process at the extent of reaction larger than 0.12, and hence higher temperatures (t > 70 °C), can be fitted into all models except A2, A3, A4, and D3. Not always, the real reaction mechanism could be judge by the best-fitted model to the experimental data.

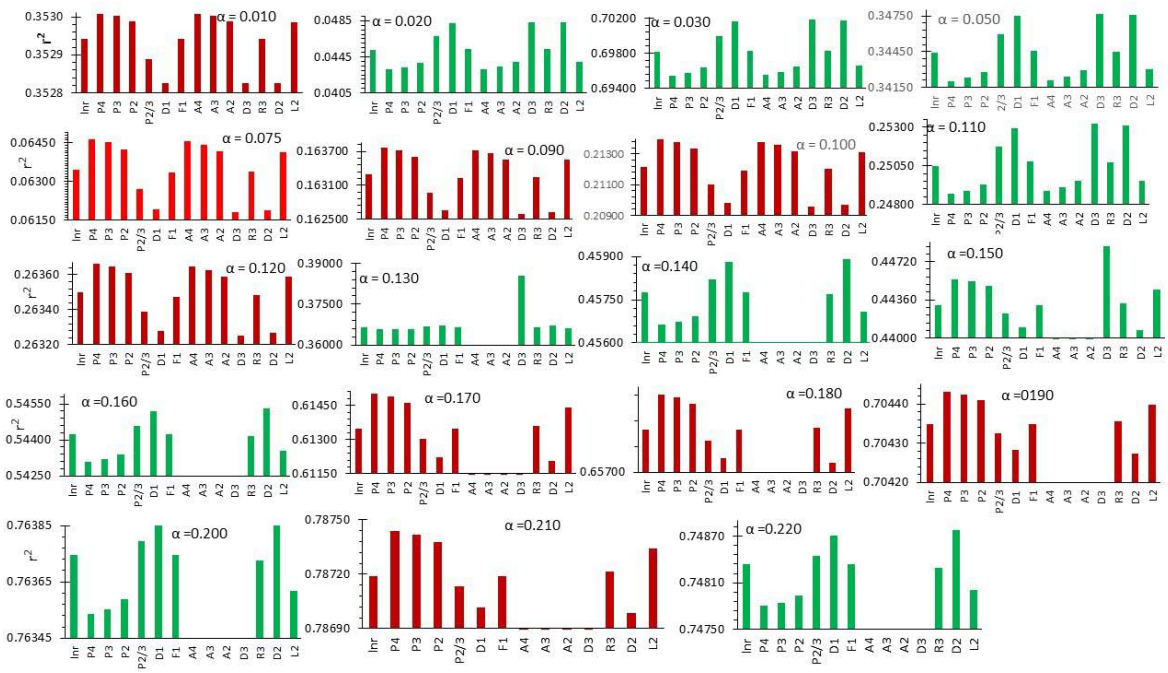

Fig. 7: Variations of the Values of r2 According to f (α) Models Enlisted in Table1.

V. Summary, Conclusions, and Remarks

Polyamide gel that hosts the hygroscopic calcium chloride was made of acrylamide combined with N, N'-methylenebisacrylamide in the presence of carbon nanotubes (DHG). DHG absorbs moisture from the environment at lower temperatures and desorbs water at a slightly higher temperature (t > 40 °C). Here, the relationship between thermosensitive and water desorption of the DHG was reported.

The crosslinked hydrogel network maintains the deliquescent solution in a solid form. Thus its water harvesting capacity is enhanced.

In this study, 14 most used reaction models, tabulated in Table 1, were analyzed, and all provided very similar results. The estimated amount of Ea was independent of the model, with a standard deviation of less than 0.07 kJmol-1. Therefore, the data from all models fall on top of each other in the corresponding graphs as shown in Fig 5 (a).

Acknowledgements

The author acknowledges the support of the United States Department of Agriculture (USDA), National Institute of Food and Agriculture, Evans-Allen project number SCX-311-29-21. Also, we express our gratitude to Dr. Salley, Dr. L. Whitesides, and their teams for their constant encouragement and support. Any opinions, findings, conclusions, or recommendations expressed in this material are those of the authors and do not necessarily reflect those of the Funding Agency.

Conflict of Interest

On behalf of all authors, the corresponding author states that there is no conflict of interest.

Biblography

1. Igor Shiklomanov's chapter The World's Water; Gleick, P.H., Ed.; Island Press/Center for Resource Economics: Washington, DC, 1993; ISBN 978-1-59 726-421-1.
2. Siddiqui, M. A.; Azam, M.A.; Khan, M.M.; Iqbal, S.; Khan, M. U.; Raffat, Y. Current Trends on Extraction of Water from Air: An Alternative Solution to Water Supply. International Journal of Environmental Science and Technology 2022, doi: 10.1007/s137 62-022-03965-8.
3. Hamidi, N.; Gargallo, L.; Whitesides, L. Water and Atmospheric Water Generation in Recent Progress in Science and Technology Vol. 5. In; Afefy, Prof. H. M., Ed.; B P International (a part of Sciencedomain International), 2023; Vol. 5, pp. 43–67 ISBN 97881 19102136.
4. Khalil, B.; Adamowski, J.; Shabbir, A.; Jang, C.; Rojas, M.; Reilly, K.; Ozga-Zielinski, B. A Review: Dew Water Collection from Radiative Passive Collectors to Recent Developments of Active Collectors. Sustain Water Resour Manag 2016, 2, 71–86, doi: 10.1007/s40899-015-0038-z.
5. Jarimi, H.; Powell, R.; Riffat, S. Review of Sustainable Methods for Atmospheric Water Harvesting. International Journal of Low-Carbon Technologies 2020, 15, 253–276.
6. Azeem, M.; Noman, M.T.; Wiener, J.; Petru, M.; Louda, P. Structural Design of Efficient Fog Collectors: A Review. Environ Technol Innov 2020, 20, 101169, doi:10.1016/j.eti.2020.101169.
7. Meza, I.; Siebert, S.; Döll, P.; Kusche, J.; Herbert, C.; Eyshi Rezaei, E.; Nouri, H.; Gerdener, H.; Popat, E.; Frischen, J.; et al. Global-Scale Drought Risk Assessment for Agricultural Systems. Natural Hazards and Earth System Sciences 2020, 20, 695–712, doi: 10.5194/nhess-20-695-2020.
8. Boretti, A.; Rosa, L. Reassessing the Projections of the World Water Development Report. NPJ Clean Water 2019, 2, 15, doi: 10.1038/s41545-019-0039-9.
9. Ciampi, M. 'Water Divide' in the Global Risk Society. International Review of Sociology 2013, 23, 243–260, doi: 10.1080/03906701.2013.771468.
10. Zhou, X.; Lu, H.; Zhao, F.; Yu, G. Atmospheric Water Harvesting: A Review of Material and Structural Designs; American Chemical Society, 2020; Vol. 2, pp. 671–684.
11. Rubin, S.J. Water Costs and Affordability in the United States: 1990 to 2015. J Am Water Works Assoc 2018, 110, 48–52, doi:10.1002/awwa.1062.
12. Spicer, N.; Parlee, B.; Chisaakay, M.; Lamalice, D. Drinking Water Consumption Patterns: An Exploration of Risk Perception and Governance in Two First Nations Communities. Sustainability 2020, 12, 6851, doi: 10.3390/su12176851.
13. FAO The State of the World's Land and Water Resources for Food and Agriculture – Systems at Breaking Point (SOLAW 2021); FAO, 2021; ISBN 978-92-5-135327-1.
14. Fresán, U.; Marrin, D.; Mejia, M.; Sabaté, J. Water Footprint of Meat Analogs: Selected Indicators According to Life Cycle Assessment. Water (Basel) 2019, 11, 728, doi: 10.3390/w11040728.
15. Mekonnen, M.M.; Gerbens-Leenes, W. The Water Footprint of Global Food Production. Water (Basel) 2020, 12, 2696, doi: 10.3390/w121 02696.
16. Vanham, D.; Mekonnen, M.M. The Scarcity-Weighted Water Footprint Provides Unreliable Water Sustainability Scoring. 2021, 756, 143992, doi: 10.1016/j.scitotenv.2020.143992.
17. Guo, Y.; Zhou, X.; Zhao, F.; Bae, J.; Rosenberger, B.; Yu, G. Synergistic Energy Nanoconfinement and Water Activation in Hydrogels for Efficient Solar Water Desalination. ACS Nano 2019, 13, 7913–7919, doi: 10.1021/acsnano.9b02301.
18. Xi, Z.; Li, S.; Yu, L.; Yan, H.; Chen, M. All-Day Freshwater Harvesting by Selective Solar Absorption and Radiative Cooling. ACS Appl Mater Interfaces 2022, 14, 26255– 26263, doi: 10.1021/acsami.2c05 409.
19. Xu, J.; Zhang, J.; Fu, B.; Song, C.; Shang, W.; Tao, P.; Deng, T. All-Day Freshwater Harvesting through Combined Solar-Driven Interfacial Desalination and Passive Radiative Cooling. ACS Appl Mater Interfaces 2020, 12, 47612–47622, doi: 10.1021/ acsami.0c14773.

20. Mekonnen, M.M.; Hoekstra, A.Y. Four Billion People Facing Severe Water Scarcity. Sci Adv 2016, 2, doi: 10.1126/sciadv.1500323.
21. Pérez-González, A.; Urtiaga, A.M.; Ibáñez, R.; Ortiz, I. State of the Art and Review on the Treatment Technologies of Water Reverse Osmosis Concentrates. Water Res 2012, 46, 267–283, doi:10.1016/j.watres.2011.10.046.
22. D. Mahan; O. Waissbluth; D. Caceres Carcinogenic and Non-Carcinogenic Health Risks of Arsenic Exposure in Drinking Water in the Rural Environment. Global J. Environ. Sci. Manage. 2020, 6, 165–174.
23. Zhang, Y.; Zhu, W.; Zhang, C.; Peoples, J.; Li, X.; Felicelli, A.L.; Shan, X.; Warsinger, D.M.; Borca-Tasciuc, T.; Ruan, X.; et al. Atmospheric Water Harvesting by Large-Scale Radiative Cooling Cellulose-Based Fabric. Nano Lett 2022, 22, 2618–2626, doi:10.1021/acs.nanolett.1c04143.
24. Anderson, P.J.; Miller, A.D.; O'malley, K.A.; Ceridon, M.L.; Beck, K.C.; Wood, C.M.; Wiste, H.J.; Mueller, J.J.; Johnson, J.B.; Johnson, B.D. Incidence and Symptoms of High Altitude Illness in South Pole Workers: Antarctic Study of Altitude Physiology (ASAP). Clin Med Insights Circ Respir Pulm Med 2011, 5, CCRPM.S6882, doi: 10.4137/CCRPM.S6882.
25. Cashman, S.; Ma, C. (Xin); Garland, J.; Morelli, B. Overview of Resource Recovery- Based Sustainable Water Systems: Life Cycle Assessment Updates from US EPA's Safe and Sustainable Water Research Program; 2018;
26. Ma, X.; Zhao, X.; Zhang, Y.; Liu, K.; Yang, H.; Li, J.; Akhlaghi, Y.G.; Liu, H.; Han, Z.; Liu, Z. Combined Rankine Cycle and Dew Point Cooler for Energy Efficient Power Generation of the Power Plants - A Review and Perspective Study. Energy 2022, 238, 121688, doi: 10.1016/j.energy.2021.121688.
27. Park, H.; Haechler, I.; Schnoering, G.; Ponte, M.D.; Schutzius, T. M.; Poulikakos, D. Enhanced Atmospheric Water Harvesting with Sunlight-Activated Sorption Ratcheting. ACS Appl Mater Interfaces 2022, 14, 2237–2245, doi: 10.1021/acsami.1c18852.
28. Liu, X.; Beysens, D.; Bourouina, T. Water Harvesting from Air: Current Passive Approaches and Outlook; American Chemical Society, 2022; Vol. 4, pp. 1003–1024.
29. Li, R.; Shi, Y.; Alsaedi, M.; Wu, M.; Shi, L.; Wang, P. Hybrid Hydrogel with High Water Vapor Harvesting Capacity for Deployable Solar-Driven Atmospheric Water Generator. 2018, 52, 11367–11377, doi: 10.1021/acs.est.8b02852.
30. Kim, S.; Choi, H. Switchable Wettability of Thermoresponsive Core–Shell Nanofibers for Water Capture and Release. ACS Sustain Chem Eng 2019, 7, 19870–19879, doi: 10.1021/acssuschemeng.9b05273.
31. Diouf, D.; Darmanin, T.; Diouf, A.; Dieng, S.Y.; Guittard, F. Surface Nanostructuration and Wettability of Electrodeposited Poly(3,4-Ethylenedioxypyrrole) and Poly (3,4- Propylenedioxypyrrole) Films Substituted by Aromatic Groups. ACS Omega 2018, 3, 8393–8400, doi:10.1021/acsomega.8b00871.
32. Thakur, N.; Sargur Ranganath, A.; Sopiha, K.; Baji, A. Thermoresponsive Cellulose Acetate-Poly(N-Isopropylacrylamide) Core-Shell Fibers for Controlled Capture and Release of Moisture. ACS Appl Mater Interfaces 2017, 9, 29224–29233, doi: 10.1021/acsami.7b07559.
33. Na, K.; Lee, K.H.; Lee, D.H.; Bae, Y.H. Biodegradable Thermo-Sensitive Nanoparticles from Poly(l-Lactic Acid)/Poly(Ethylene Glycol) Alternating Multi-Block Copolymer for Potential Anti-Cancer Drug Carrier. European Journal of Pharmaceutical Sciences 2006, 27, 115–122, doi:10.1016/j.ejps.2005.08.012.
34. Yang, M.; Wang, S.-Q.; Liu, Z.; Chen, Y.; Zaworotko, M.J.; Cheng, P.; Ma, J.-G.; Zhang, Z. Fabrication of Moisture-Responsive Crystalline Smart Materials for Water Harvesting and Electricity Transduction. J Am Chem Soc 2021, 143, 7732–7739, doi: 10.1021/jacs. 1c01831.
35. Echeverria, C.; Fernandes, S.; Godinho, M.; Borges, J.; Soares, P. Functional Stimuli- Responsive Gels: Hydrogels and Microgels. Gels 2018, 4, 54, doi: 10.3390/gels4020054.
36. Wei, M.; Gao, Y.; Li, X.; Serpe, M.J. Stimuli-Responsive Polymers and Their Applications. Polym Chem 2017, 8, 127–143, doi:10.1039/C6PY01585A.
37. Guo, Y.; Bae, J.; Fang, Z.; Li, P.; Zhao, F.; Yu, G. Hydrogels and Hydrogel-Derived Materials for Energy and Water Sustainability. Chem Rev 2020, 120, 7642–7707.
38. Hanikel, N.; Prévot, M.S.; Yaghi, O.M. MOF Water Harvesters. Nat Nanotechnol 2020, 15, 348–355, doi: 10.1038/s41565-020-0673-x.
39. Nguyen, H.L.; Gropp, C.; Hanikel, N.; Möckel, A.; Lund, A.; Yaghi, O.M. Hydrazine- Hydrazide-Linked Covalent Organic Frameworks for Water Harvesting. ACS Cent Sci 2022, doi: 10.1021/acscentsci.2c00398.
40. LaPotin, A.; Kim, H.; Rao, S.R.; Wang, E.N. Adsorption-Based Atmospheric Water Harvesting: Impact of Material and Component Properties on System-Level Performance. Acc Chem Res 2019, 52, 1588–1597, doi:10.1021/acs.accounts.9b00062.
41. Gido, B.; Friedler, E.; Broday, D.M. Liquid-Desiccant Vapor Separation Reduces the Energy Requirements of Atmospheric Moisture Harvesting. Environ Sci Technol 2016, 50, 8362–8367, doi: 10.1021/acs.est.6b01280.

42. Mulchandani, A.; Edberg, J.; Herckes, P.; Westerhoff, P. Seasonal Atmospheric Water Harvesting Yield and Water Quality Using Electric-Powered Desiccant and Compressor Dehumidifiers. Science of The Total Environment 2022, 825, 153966, doi: 10.1016/j.scitotenv.2022.153966.
43. Mehta, J.R.; Desai, T.K.; Patel, A.K.; Diyora, H.B.; Rabadiya, A.S. Preliminary Investigations on a Novel Rotating Media Liquid-Air Contacting Device without Liquid Pool. In Proceedings of the Energy Procedia; Elsevier Ltd, March 1 2017; Vol. 109, pp. 167–173.
44. Entezari, A.; Ejeian, M.; Wang, R. Super Atmospheric Water Harvesting Hydrogel with Alginate Chains Modified with Binary Salts. ACS Mater Lett 2020, 2, 471–477, doi: 10.1021/acsmaterialslett.9b00315.
45. Liu, X.; Wang, X.; Kapteijn, F. Water and Metal-Organic Frameworks: From Interaction toward Utilization. Chem Rev 2020, 120, 8303–8377.
46. Feng, R.; Xu, C.; Song, F.; Wang, F.; Wang, X.-L.L.; Wang, Y.-Z.Z. A Bioinspired Slippery Surface with Stable Lubricant Impregnation for Efficient Water Harvesting. 2020, 12, 12373–12381, doi: 10.1021/acsami.0c00234.
47. Zhu, S.-Q.; Feng, R.; Liang, Z.-H.; Wang, X.-L.; Wang, Y.-Z.; Song, F. Efficient Water Harvesting Enabled by Porous Architecture-Containing Hybrid Surfaces. Ind Eng Chem Res 2022, doi: 10.1021/acs.iecr.2c00717.
48. Pérez-Maqueda, L.A.; Criado, J.M.; Sánchez-Jiménez, P.E. Combined Kinetic Analysis of Solid-State Reactions: A Powerful Tool for the Simultaneous Determination of Kinetic Parameters and the Kinetic Model without Previous Assumptions on the Reaction Mechanism. J Phys Chem A 2006, 110, 12456–12462, doi: 10.1021/jp064792g.
49. Lapčík, L.; Kellö, V.; Očadlík, J. Kinetic Study of Dissolution of Poly (Vinyl Chloride) in Tetrahydrofuran, Cyclohexanone, Cyclopentanone, and AT, IV-Dimethylformamide.
50. Krongauz, V. V.; Lee, Y. P.; Bourassa, A. Kinetics of Thermal Degradation of Poly (Vinyl Chloride): Thermogravimetry and Spectroscopy. In Proceedings of the Journal of Thermal Analysis and Calorimetry; October 2011; Vol. 106, pp. 139–149.
51. Blazevska-Gilev, J. Formal Kinetic Analysis of PVC Thermal Degradation; 2010; Vol. 45.
52. Alwaan, I.M. Kinetics of Thermal Degradation of Recycled Polyvinyl Chloride Resin. International Journal of Chemical Engineering 2014, doi: 10.1155/2014/701092.
53. Hamidi, N. Kinetics Study of the Thermal Decomposition of Post-Consumer Poly (Ethylene Terephthalate) in an Argon Atmosphere. Journal of Macromolecular Science, Part B: Physics 2019, 58, doi:10.1080/00222348.2019.1576102.
54. Khoshnoud, P.; Abu-Zahra, N. Kinetics of Thermal Decomposition of PVC/Fly Ash Composites. International Journal of Polymer Analysis and Characterization 2018, 23, 170–180, doi:10.1080/1023666X.2017.1404668.
55. Xu, M.; Cao, C.; Hu, H.; Ren, Y.; Guo, G.; Gong, L.; Zhang, J.; Zhang, T.; Yao, H. Perspective on the Disposal of PVC Artificial Leather via Pyrolysis: Thermodynamics, Kinetics, Synergistic Effects and Reaction Mechanism. Fuel 2022, 327, 125082, doi:10.1016/j.fuel.2022.125082.
56. Indo, R. Decomposition of Polyvinyl Chloride, Polypropylene and Melamine Using Thermo--gravimetric Analyzer Analyzer. 2019, 14.
57. Park, H.-J. Evaluation of the Activation Energy of Chlorinated Poly Vinyl Chloride (CPVC) Using Thermogravimetric Analysis. Fire science and engineering 2019, 33, 1–6, doi: 10.7731/kifse.2019.33.1.001.
58. Peterson, J.D.; Vyazovkin, S.; Wight, C.A. Kinetics of the Thermal and Thermo-Oxidative Degradation of Polystyrene, Polyethylene and Poly (Propylene); 2001; Vol. 202;.
59. Vyazovkin, S.; Burnham, A.K.; Favergeon, L.; Koga, N.; Moukhina, E.; Pérez-Maqueda, L.A.; Sbirrazzuoli, N. ICTAC Kinetics Committee Recommendations for Analysis of Multi-Step Kinetics. Thermochim Acta 2020, 689, 178597, doi: 10.1016/j.tca.2020.178597.
60. Dong, Z.; Yang, Y.; Cai, W.; He, Y.; Chai, M.; Liu, B.; Yu, X.; Banks, S.W.; Zhang, X.; Bridgwater, A. V.; et al. Theoretical Analysis of Double Logistic Distributed Activation Energy Model for Thermal Decomposition Kinetics of Solid Fuels. Ind Eng Chem Res 2018, 57, 7817–7825, doi:10.1021/acs.iecr.8b01527.
61. Atkins, P.; De Paula, J. Physical Chemistry, 9th Edition ; 9th ed.; W. H. Freeman, 2009: New York, NY, 2009.
62. Sbirrazzuoli, N. Advanced Isoconversional Kinetic Analysis for the Elucidation of Complex Reaction Mechanisms: A New Method for the Identification of Rate-Limiting Steps. Molecules 2019, 24, 1683, doi: 10.3390/molecules24091683.
63. Ding, J.; Zhang, X.; Hu, D.; Ye, S.; Jiang, J. Model-Free Kinetic Determination of Pre- Exponential Factor and Reaction Mechanism in Accelerating Rate Calorimetry. Thermochim Acta 2021, 702, 178983, doi: 10.1016/j.tca.2021.178983.
64. Sbirrazzuoli, N. Determination of Pre-Exponential Factors and of the Mathematical Functions f(α) or G(α) That Describe the Reaction Mechanism in a Model-Free Way. Thermochim Acta 2013, 564, 59–69, doi: 10.1016/j.tca.2013.04.015.
65. Castellan, G.W. Physical Chemistry; Third.; Addison-Wesley Publishing Company: Reading, Massachusetts, 1983; ISBN ISBN 0-201-10386-9.